

Article

# CuZnSn(S<sub>x</sub>Se<sub>1-x</sub>)<sub>4</sub> Solar Cell Prepared by the Sol-Gel Method Following a Modified Three-Step Selenization Process

Xunan Shen <sup>1,2,3</sup>, Chengchun Tang <sup>1,3,\*</sup>, Chao Zhang <sup>2,\*</sup>, Guanda Li <sup>4</sup>, Yue Zhao <sup>2</sup>, Wei Li <sup>5</sup>, Guifeng Chen <sup>1</sup> and Tie Yang <sup>6,\*</sup> 

<sup>1</sup> School of Materials Science and Engineering, Hebei University of Technology, Tianjin 300130, China; xnshen@nklps.org (X.S.); cgfchen@hebut.edu.cn (G.C.)

<sup>2</sup> Science and Technology on Power Sources Laboratory, Tianjin Institute of Power Sources, Tianjin 300130, China; yzhao@nklps.org

<sup>3</sup> Hebei Key Laboratory of Boron Nitride Micro and Nano Materials, Hebei University of Technology, Tianjin 300130, China

<sup>4</sup> School of Chemical Engineering, Dalian University of Technology, Dalian 116024, China; liguanda@mail.dlut.edu.cn

<sup>5</sup> School of Electrical and Electronic Engineering, Tianjin Key Laboratory of Film Electronic & Communication Devices, Tianjin University of Technology, Tianjin 300191, China; cliwei618@yeah.net

<sup>6</sup> School of Physical Science and Technology, Southwest University, Chongqing 400715, China

\* Correspondence: tangcc@hebut.edu.cn (C.T.); czhang@nklps.org (C.Z.); yangtie@swu.edu.cn (T.Y.)

Received: 19 August 2019; Accepted: 6 September 2019; Published: 11 September 2019



**Abstract:** In current work, Cu<sub>2</sub>ZnSn(S,Se)<sub>4</sub> thin films have been prepared by the sol-gel method based on dimethyl sulfoxide solution followed by a modified three-step selenization process. The key process of this method is to divide the Se evaporation and annealing into two different stages: employ a thermal cracking Se source in the Se evaporation stage and an above-atmospheric pressure in the annealing process. The morphological, structural, elemental distributional, and photovoltaic properties of Cu<sub>2</sub>ZnSn(S,Se)<sub>4</sub> thin films prepared with the three-step selenization process were systematically investigated. It was found that through this modified selenization process, the formations of secondary phases (ZnSe, CuSnSe<sub>3</sub>) and a fine-grain bottom layer, which usually exists in the traditional one-step selenization process, were effectively suppressed. These improvements could further reduce the carrier recombination and improve the solar cell performance. The best solar cell is obtained with a short-circuit current density of 28.16 mA/cm<sup>2</sup>, open-circuit voltage of 404.91 mV, fill factor of 62.91%, and a power conversion efficiency of 7.17% under air mass 1.5 (100 mW/cm<sup>2</sup>) illumination.

**Keywords:** CZTSSe solar cell; sol-gel method; selenization; thermal cracking Se; above-atmospheric pressure; secondary phases

## 1. Introduction

Second generation thin film solar cells such as cadmium telluride (CdTe) and copper indium gallium diselenide (CIGS) are currently attracting a lot of attention for their low-capital cost and high efficiency [1,2]. However, concerns about the use of expensive and toxic elements (In and Cd) have led researchers to seek out an alternative material system [3]. Among different candidates, Cu<sub>2</sub>ZnSn(S,Se)<sub>4</sub> (CZTSSe) might be a promising material owing to its abundance, low cost, and environmentally friendly properties [4]. Additionally, CZTSSe has a high optical absorption coefficient (>10<sup>4</sup> cm<sup>-1</sup>) and a direct band gap with high tunability by simply changing the S/Se ratio [5].

Up to now, several methods have been proposed to fabricate the CZTSSe solar cells, such as sputtering deposition [6], co-evaporation [7], electrodeposition [8], pulsed laser deposition [9],

solution ink printing [10], and the sol-gel method [11,12]. Until now, the highest obtained power conversion efficiency of the CZTSSe solar cell is 12.6% using a type of pure hydrazine-based molecular solution [13]. Conventionally, for the CZTSSe solar cell preparation based on solution methods, a post-selenization is commonly needed. Thus, this process has been investigated extensively [14,15]. For example, Zhao et al. have studied the effect of annealing time and heating rate in ambient Se vapour [16]; Yao et al. prepared CZTSSe solar cells by selenization at a low pressure with Se and SnSe<sub>2</sub> sources [17]; Xin et al. adopted the absorber selenization process under high argon pressure [18]. Moreover, the selenization process usually results in the formation of a bi-layer structure with bi-modal grain size, which consists of a rough-grain upper layer and a fine-grain bottom layer [11,16,19]. The fine-grain underlayer contains various residual organic solvent and secondary phases (ZnSe, ZnS, SnSe<sub>2</sub>, SnS, Cu<sub>2</sub>Se, Cu<sub>2</sub>S, CuSnSe<sub>3</sub> et al.), which could greatly impact the performance of CZTSSe solar cells [20]. In general, the formation of the bi-layer structure is due to that, in the annealing process, the Se vapour can not fully reach the bottom of the CZTS precursor layer, which is caused by the restrained further diffusion of Se atoms from the crystallized grain in the upper layer. In order to effectively reduce this bi-layer structure and improve the crystal quality, Jong-Ok Jeon applied the thermal annealing process at high Se pressure and successfully reduced the thickness of the fine-grain underlayer [21]. However, selenization at high Se pressure is highly likely to introduce a thick MoSe<sub>2</sub> layer formation, which in turn degrades the performance of the solar cell device [22]. Therefore, an effective selenization process is urgently needed to further optimize the preparation of CZTSSe solar cells based on the solution method and enhance their performance.

In this study, we designed and proposed a new three-step selenization process with respect to the conventional one-step process. In our selenization process, we divided the Se evaporation and annealing into two different stages to obtain a large grain layer without other secondary phases. In the Se evaporation stage, a thermal cracking Se source was used to disperse the Se atoms among the precursor film. Then, in the annealing stage, an above-atmospheric pressure was adopted to reduce the loss of Sn and enhance Se diffusion. The structural morphology, elemental distribution, and photovoltaic properties of the prepared CZTSSe thin film with the three-step selenization process were systematically studied. As we anticipated, a better crystal quality was obtained with effective suppression of other second phases. In the end, CZTSSe solar cells prepared with our proposed method showed much better performance with greatly improved efficiency of 7.17% under air mass 1.5 (100 mW/cm<sup>2</sup>) illumination.

## 2. Experimental Details

The precursor solution was prepared by successively dissolving 10 mmol Cu(CH<sub>3</sub>COO)<sub>2</sub> and 6.7 mmol SnCl<sub>2</sub> in 80 mL dimethyl sulfoxide (DMSO) solution with stirring overnight. Then, 7 mmol ZnCl<sub>2</sub> and 38.8 mmol thiourea were added and it was further stirred for another two hours to obtain a clear yellow solution. All chemicals were 99% purity and purchased from Aladdin (Shanghai, China).

The CZTS precursor films were spin-coated onto the molybdenum coated soda-lime glass substrates at a speed of 1540 rpm for 50 s and were then immediately annealed on a 540 °C hotplate for 5 min. This process was repeated seven times. All the processes were carried out in an argon filled glovebox system with oxygen and water less than 10 ppm, including all the solution preparation, thin film spin-coating, and annealing.

In order to complete the preparation of the CZTSSe film, a three-step selenization process was carried out. In the first step, the precursor film was put into a vacuum chamber under 10–3 Pa background pressure. Without argon flow, the sample without substrate heating (<70 °C) was annealed for 5 min under an 800 °C thermal cracking Se source. In this step, the Se atoms could diffuse into the CZTS precursor and did not react with CZTS particles. For the second step, the annealed CZTS precursor film was put into a graphite box (Bohua Tec, Tianjin, China) with 50 mg Se pellets and selenized at 530 °C for 10 min in a furnace under an above-atmospheric pressure (1.2 × 10<sup>5</sup> Pa) without argon flow. During the third step, the furnace was kept at 320 °C for another 10 min to

eliminate the residual Se on the surface of the film and was naturally cooled down to room temperature. For comparison, one control sample was prepared by the widely applied one-step selenization process [23], and the temperature and annealing time were optimized according to our previous work. The specific process was that the CZTS precursor film was put in a graphite box with 200 mg Se pellets and selenized at 530 °C for 20 min in a furnace under argon gas flow and was then cooled down to room temperature naturally.

After the selenization process, a 60 nm CdS layer was deposited on the CZTSSe film by chemical bath deposition (CBD). Then, by the RF sputtering method, a 50 nm i-ZnO layer and 350 nm Al-doped ZnO layer were deposited sequentially. Finally, the solar cell fabrication was finished by e-beam evaporation of Ni–Al top electrode using a shadow mask. Each sample of  $4 \times 4 \text{ cm}^2$  contained 12 sub solar cells and each one was  $0.38 \text{ cm}^2$ .

The morphological properties of the thin films were examined with a Hitachi S4800 field emission scanning electron microscope (FE-SEM) (HITACHI, Tokyo, Japan). X-ray diffraction (XRD) (Rigaku, Tokyo, Japan) patterns were measured with a M18XHF-SRA diffractometer (Rigaku, Tokyo, Japan) with monochromatic Cu K $\alpha$  radiation. Raman spectrum (Renishaw, London, UK) was analyzed with a Nd-YAG 532 nm laser in a Horiba Jobin Yvon T64000 spectroscopy (Renishaw, London, UK). The elemental composition measurements were carried out with Thermal i-cap 6300 inductively coupled plasma mass spectrometry (ICP) (Thermal, San Francisco, USA). The depth profiles of the elements were obtained by secondary ion mass spectrometry (SIMS, IMS-4F) (Cameca, Paris, France). Current-voltage (J-V) measurements were performed using a Keithley 2400 source-measure unit under 100 mW/cm<sup>2</sup> simulated AM1.5G illumination from a xenon arc lamp with a AM1.5G filter (Daheng Tec, Beijing, China).

### 3. Results and Discussions

The elemental compositions of the CZTS precursor film and selenized CZTSSe films prepared with both the conventional one-step and our modified three-step process are listed in Table 1. By comparing the CZTSSe films fabricated by the one-step and three-step selenization process, the sample with the three-step selenization process shows both a lower Zn/Sn and Cu/(Zn + Sn) ratio. Besides, it is also found that the CZTSSe film with the three-step selenization process has a higher residual S content. Based on previous works [8,24,25], the loss of Sn element is mainly caused by the evaporation of SnS and SnSe phases and the formation of various defects and composition segregation. This phenomenon could hamper the performance of CZTSSe solar cells [25]. Herein, our result of S content increase in the sample prepared with the three-step process indicates that this modified three-step selenization process could effectively suppress the loss of Sn and S elements and secondary phase formation.

**Table 1.** The measured chemical compositions of the CZTS precursor film and CZTSSe films.

Sample	Element Compositions (%)					Composition Ratios		
	Cu	Zn	Sn	S	Se	Cu/(Zn + Sn)	Zn/Sn	
Precursor film	23.81	15.55	14.86	45.78	-	0.78	1.05	
Selenide films	One-step	20.94	13.92	11.71	5.13	48.31	0.82	1.19
	Three-step	21.07	13.97	12.03	5.79	47.15	0.81	1.16

Figure 1 shows the FE-SEM images of the CZTS precursor and CZTSSe thin films. Figure 1(a–f) correspond the top surface and cross-sectional images of the CZTS precursor and the CZTSSe films with the one-step and three-step selenization process, respectively. As shown in Figure 1(a), there are numerous holes and cracks in the surface of the CZTS precursor film, and these defects provide the channel for the diffusion of Se atoms. By comparing the images of CZTSSe films with the one-step and three-step selenization process, we can observe that the crystallinity of CZTSSe films with the three-step selenization process is enhanced with a larger grain size. Further, both of the two samples

show a bi-layer structure. As explained before, the formation of the bi-layer structure is due to the Se vapour reacting with the upper CZTS particles and translating to a CZTSSe crystallized grain layer. Further, the upper CZTSSe layer might restrain the further diffusion of Se atoms to the CZTS underlayer. The absence of Se causes numerous second phase formations. A closer look shows that the film with the one-step selenization process shows a fine-grain bottom layer. Whereas, the film with the three-step selenization process does not have a fine-grain layer; both the bottom and top layers show a large grain structure. This fine-grain layer usually contains a lot of secondary phases, such as ZnS(e) and SnS(e), which could hinder the carrier transportation. This different bottom layer morphology from the three-step process is owing to the fact that Se atoms can diffuse through the CZTS precursor film more homogeneously without the substrate heating in the first step.

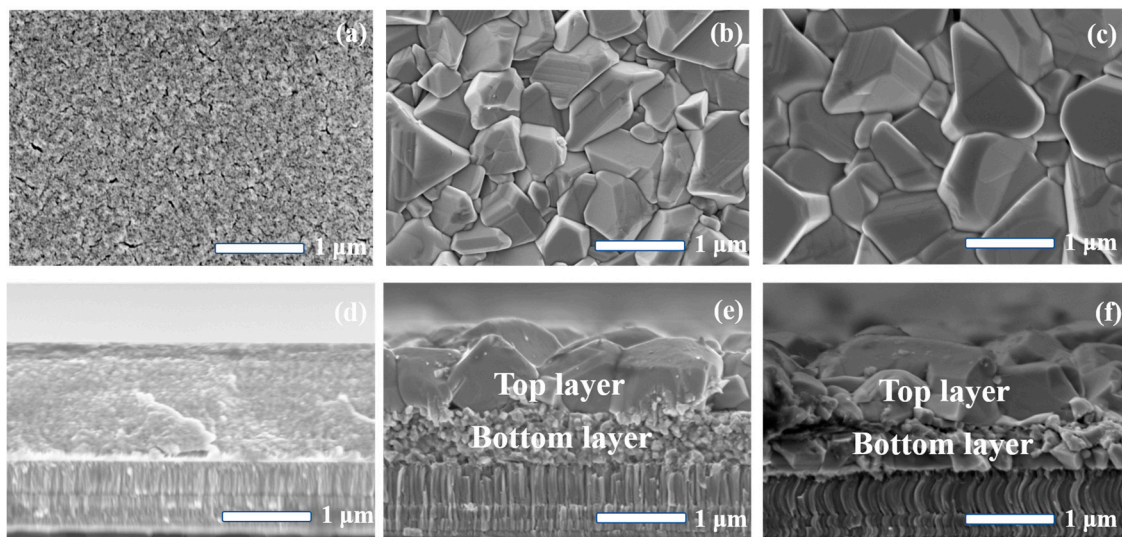


**Figure 1.** Surface and cross-sectional SEM images of (a,d) CZTS precursor film, (b,e) CZTSSe film with the one-step selenization process, (c,f) CZTSSe film with the three-step selenization process.

Figure 2 shows the XRD patterns of CZTSSe thin films prepared with both the one-step and three-step selenization process. Both the samples have several prominent reflections along the (112), (211), (204), and (312) planes, which verifies the formation of the CZTSSe structures [PDF#97-009-5117]. In comparison, the (112) peak of the CZTSSe thin films with the three-step selenization process exhibits a much higher intensity than the sample with the one-step selenization process. The size of the crystallites was precisely calculated by the Scherrer equation according to the location and full width at half maximum (FWHM) of the main diffraction (112) peak [26]:

$$D = \frac{k\lambda}{\beta \cos\theta} \quad (1)$$

where  $D$  is the size of the regions of coherent scattering;  $k$  ( $=0.89$ ) is the shape factor;  $\beta$  is the width of the diffraction peak at its half maximum; and  $\lambda$  is the wavelength of the used radiation ( $=0.15406$  nm). The obtained  $D$  values calculated by equation (1) are 212.6 nm and 343.2 nm for the CZTSSe film prepared by the one-step and three-step process, respectively. These results indicate that the crystallinity of CZTSSe film was greatly enhanced with the three-step selenization process. In the three-step selenization process, adopting an above atmospheric pressure ( $1.2 \times 10^5$  Pa) may suppress the evaporation of Se element, and a high liquid Se content may promote CZTSSe grain growth. Another apparent diffraction peak in the XRD patterns is the (101) of  $\text{MoSe}_2$  (marked by  $\blacklozenge$ ). We observe that both the two samples fabricated by the one-step and three-step selenization process have a similar  $\text{MoSe}_2$  (101) peak intensity. Further, from the SEM images, we observed that the thicknesses of the

MoSe<sub>2</sub> layers are less than 100 nm. The similar, thin MoSe<sub>2</sub> layer would not affect the performance of CZTSSe solar cells.

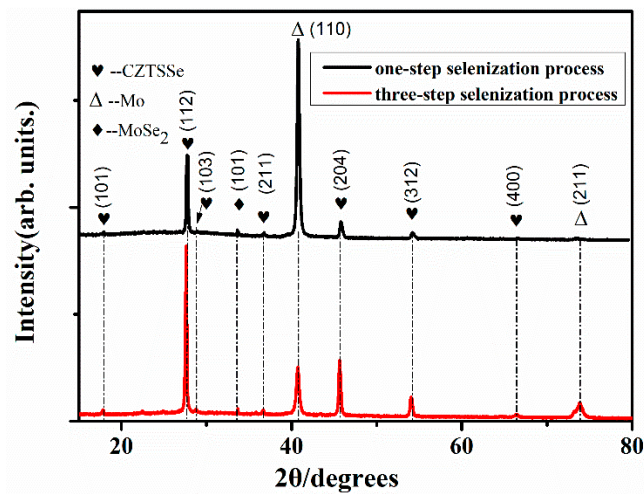


Figure 2. XRD patterns of CZTSSe film with the one-step and three-step selenization process.

Owing to the existence of some binary (cubic ZnS, ZnSe) and ternary (tetragonal Cu<sub>2</sub>SnSe<sub>3</sub>) chalcogenides, the XRD pattern is not sufficient to determine the phase purity of the synthesized materials. Thus, we also used Raman spectrum to characterize their structures. As seen in Figure 3, we find that ZnSe and CuSnSe<sub>3</sub> phases exist in the CZTSSe film with the one-step selenization process. However, these secondary phases disappear in the CZTSSe film with the three-step selenization process. The Raman results indicate that the three-step selenization process could eliminate the fine bottom layer of the CZTSSe film which contained a lot of the secondary phase (ZnSe, CuSnSe<sub>3</sub>), as also observed with the microscopic morphology in Figure 1.

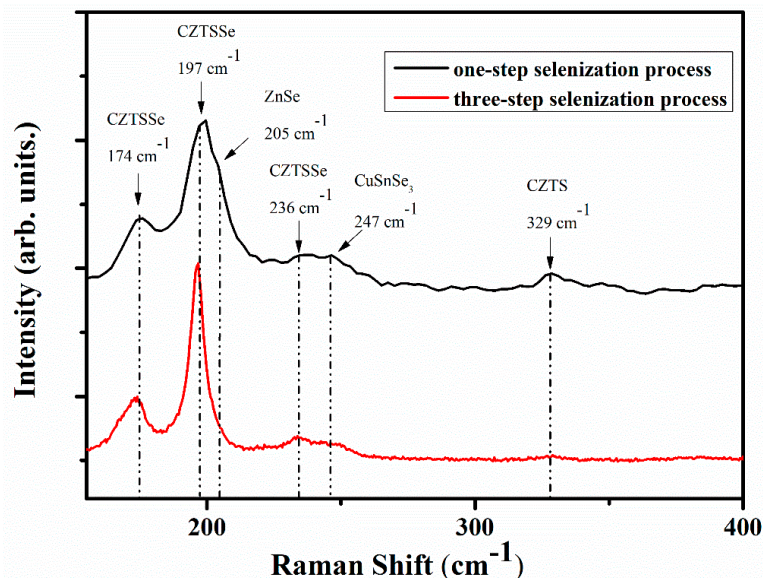
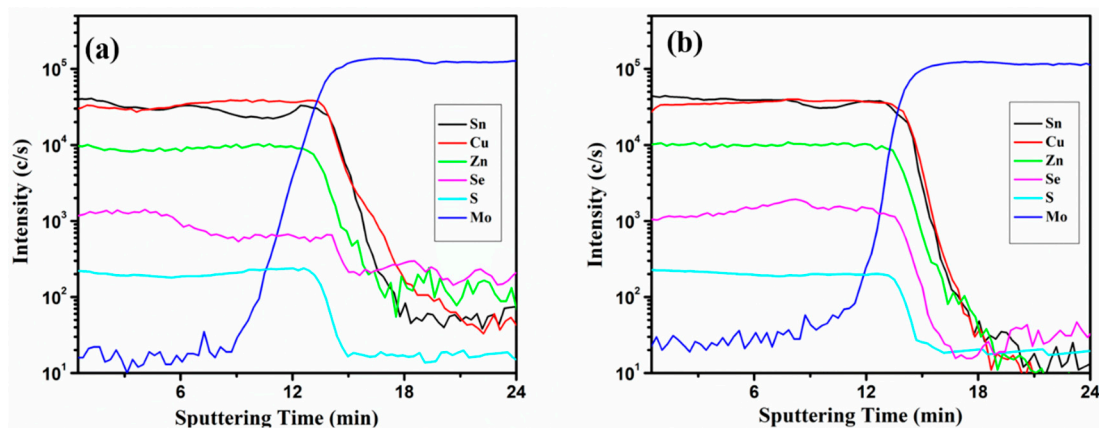


Figure 3. Raman spectrums of CZTSSe film with the one-step and three-step selenization process.

To assess the element distribution along the film thickness direction, secondary ion mass spectroscopy (SIMS) analysis was carried out. From Figure 4, we can see that the CZTSSe film with the three-step selenization process shows a uniform distribution of Se element throughout the film. The Se contents are higher in the top layer than in the bottom layer and the S is distributed

mostly homogeneously among the film. This indicates that the three-step selenization process could be beneficial for Se element diffusion.



**Figure 4.** Secondary ion mass spectroscopy (SIMS) profiles of CZTSSe films prepared by (a) one-step and (b) three-step selenization process.

In the end, the CZTSSe solar cells were prepared and the current density-voltage (J-V) curves were measured and are shown in Figure 5. The CZTSSe solar cells with the one-step selenization process exhibited an efficiency of 5.79% with an open-circuit voltage ( $V_{oc}$ ) of 370.98 mV, a short-circuit current density ( $J_{sc}$ ) of 27.61 mA/cm<sup>2</sup>, a fill factor of 56.54%. Then, the efficiency of CZTSSe solar cells with the three-step selenization process increase to 7.17% with  $V_{oc}$  of 404.91 mV,  $J_{sc}$  of 28.16 mA/cm<sup>2</sup>, and a fill factor of 62.91%. Remarkably, with the three-step selenization process, the series resistance ( $R_s$ ) decreases from 1.97  $\Omega/\square$  to 1.53  $\Omega/\square$ , and the shunt resistance ( $R_{sh}$ ) increases from 249.36  $\Omega/\square$  to 470.21  $\Omega/\square$ . The series resistance decrease is induced by the fine-grain bottom layer elimination, which has numerous secondary phases. Then, the shunt resistance increase is mainly caused by grain growth, which could reduce the channels of carrier recombination in the CZTSSe thin films. Another important point that should be noted is that the  $V_{oc}$  value is nearly elevated to 34 mV.

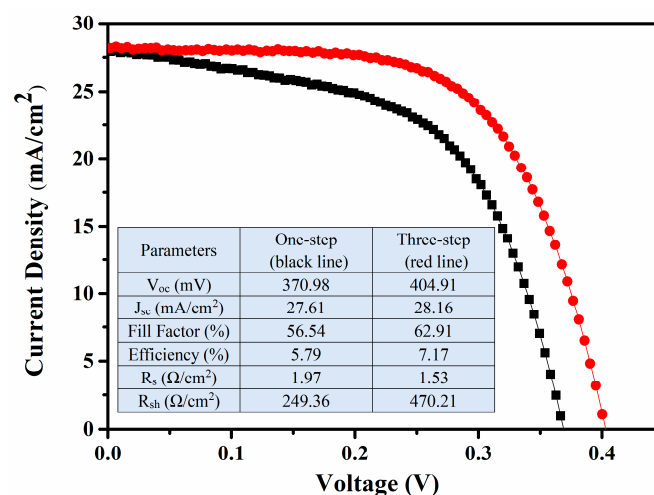


**Figure 5.** J-V characteristics of the CZTSSe solar cells prepared by the one-step and three-step selenization process.

To make the effect of the three-step selenization process on the band gap of CZTSSe solar cells clear, the external quantum efficiency (EQE) measurement was carried out and the results are shown in Figure 6. The EQE spectrum at short wavelengths (below 520 nm) indicates that the two CZTSSe solar cells with different selenization processes exhibit similar absorption originating from the

CdS/i-ZnO/AZO top layers. Further, comparable, incomplete absorptions of the absorber occur close to respective bandgaps, which is likely attributed to the insufficient thickness of the CZTSSe absorbed layer. The  $J_{sc}$  values measured by the EQE are 27.68 mA/cm<sup>2</sup> and 28.10 mA/cm<sup>2</sup> for the CZTSSe solar cell with the one-step and three-step selenization process and these results are in agreement with the J-V curves. Then, the bandgap of the absorber can be derived from the data near the band edge by plotting  $[E \times \ln(1-EQE)]^2$  versus E [27], as plotted in the inset figure. From the fitting results, it is found that the difference value of the band gap between the two selenization processes is merely 0.007 eV. Another important point that should be noted is that a gap exists between 845 nm to 1030 nm, which was caused by the difference of carrier's collection [28]. So, based on the EQE measurement, the three-step selenization process does not improve the absorber band gap. The improvements of both  $V_{oc}$  and  $J_{sc}$  are due to the decrease of the carrier recombination defects existing mainly in the grain and boundary.

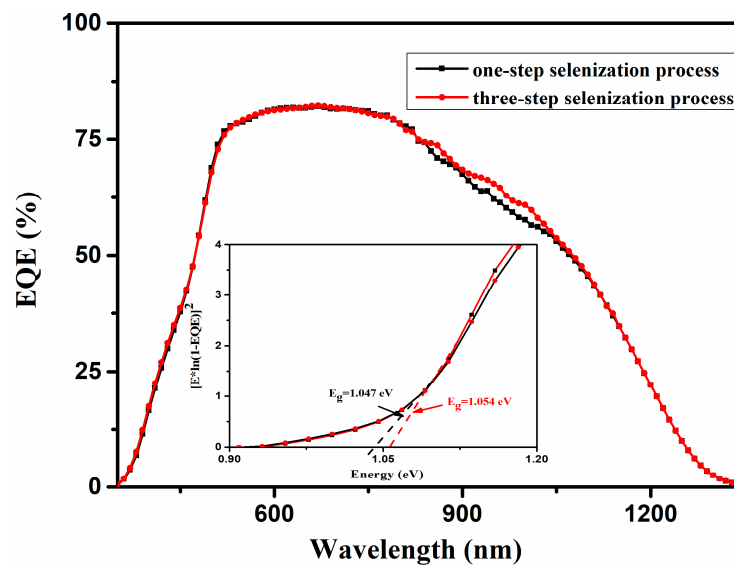


**Figure 6.** External quantum efficiency of CZTS solar cells fabricated by the one-step and three-step selenization process. Inset: Extrapolation of the band gaps from the external quantum efficiency (EQE) data.

#### 4. Conclusions

In summary, we have demonstrated that the CZTSSe thick films were fabricated with the sol-gel method followed by a modified three-step selenization process. Compared to the traditional one-step selenization process, we divided the Se evaporation and annealing into two different stages, and through adopting the above-atmospheric pressure, the formation of a homogeneous large grain layer was promoted with the secondary phases (ZnSe, CuSnSe<sub>3</sub>) effectively restrained. All these improvements could reduce the carrier recombination and then enhance the performance of CZTSSe solar cells with the efficiency increased from 5.79% to 7.17%.

**Author Contributions:** Conceptualization, X.S. and G.L.; methodology, C.Z. and T.Y.; software, Y.Z.; validation, C.T.; formal analysis, X.S. and C.T.; investigation, X.S. and T.Y.; resources, W.L. and G.C.; data curation, X.S.; writing—original draft preparation, X.S. and C.Z.; writing—review and editing, C.T. and T.Y.; visualization, G.C.; supervision, C.T. and T.Y.; project administration, X.S.; funding acquisition, W.L. and G.C.

**Funding:** This research was funded by the National Natural Science Foundation of China, grant number 61804108, 61674051, and 51871089.

**Acknowledgments:** The authors thank the anonymous reviewers for their constructive suggestions.

**Conflicts of Interest:** The authors declare no conflict of interest.

## References

1. Burst, J.M.; Duenow, J.N.; Albin, D.S.; Colegrove, E.; Reese, M.O.; Aguiar, J.A.; Jiang, C.S.; Patel, M.K.; Al-Jassim, M.M.; Kuciauskas, D.; et al. CdTe solar cells with open-circuit voltage breaking the 1 V barrier. *Nat. Energy* **2016**, *1*, 16015. [[CrossRef](#)]
2. Reinhard, P.; Buecheler, S.; Tiwari, A.N. Technological status of Cu(In,Ga)(Se,S)<sub>2</sub>-based photovoltaics. *Sol. Energy Mater. Sol. Cells* **2013**, *119*, 287–290. [[CrossRef](#)]
3. Wadia, C.; Alivisatos, A.P.; Kammen, D.M. Materials availability expands the opportunity for large-scale photovoltaics deployment. *Environ. Sci. Technol.* **2009**, *43*, 2072–2077. [[CrossRef](#)] [[PubMed](#)]
4. Zhao, W.; Wang, G.; Tian, Q.; Huang, L.; Gao, S.; Pan, D. Solution-processed Cu<sub>2</sub>ZnSn(S,Se)<sub>4</sub> thin film solar cells. *Sol. Energy Mater. Sol. Cells* **2015**, *133*, 15–20. [[CrossRef](#)]
5. Pal, K.; Singh, P.; Bhaduri, A.; Thapa, K.B. Current challenges and future prospects for a highly efficient (>20%) kesterite CZTS solar cell: A review. *Sol. Energy Mater. Sol. Cells* **2019**, *196*, 138–156. [[CrossRef](#)]
6. Li, J.; Wang, H.; Luo, M.; Tang, J.; Chen, C.; Liu, W.; Liu, F.; Sun, Y.; Han, J.; Zhang, Y. 10% Efficiency Cu<sub>2</sub>ZnSn(S,Se)<sub>4</sub> thin film solar cells fabricated by magnetron sputtering with enlarged depletion region width. *Sol. Energy Mater. Sol. Cells* **2016**, *149*, 242–249. [[CrossRef](#)]
7. Lee, Y.S.; Gershon, T.; Gunawan, O.; Todorov, T.K.; Gokmen, T.; Virgus, Y.; Guha, S. Cu<sub>2</sub>ZnSnSe<sub>4</sub> Thin-Film Solar Cells by Thermal Co-evaporation with 11.6% Efficiency and Improved Minority Carrier Diffusion Length. *Adv. Energy Mater.* **2015**, *5*, 1401372. [[CrossRef](#)]
8. Yao, L.; Ao, J.; Jeng, M.-J.; Bi, J.; Gao, S.; Sun, G.; He, Q.; Zhou, Z.; Zhang, Y.; Sun, Y.; et al. Reactive Mechanism of Cu<sub>2</sub>ZnSnSe<sub>4</sub> Thin Films Prepared by Reactive Annealing of the Cu/Zn Metal Layer in a SnSex + Se Atmosphere. *Crystals* **2018**, *9*, 10. [[CrossRef](#)]
9. Moholkar, A.V.; Shinde, S.S.; Babar, A.R.; Sim, K.-U.; Lee, H.K.; Rajpure, K.Y.; Patil, P.S.; Bhosale, C.H.; Kim, J.H. Synthesis and characterization of Cu<sub>2</sub>ZnSnS<sub>4</sub> thin films grown by PLD: *solar cells*. *J. Alloy. Compd.* **2011**, *509*, 7439–7446. [[CrossRef](#)]
10. Lin, X.; Klenk, R.; Wang, L.; Köhler, T.; Albert, J.; Fiechter, S.; Ennaoui, A.; Lux-Steiner, M.C. 11.3% efficiency Cu(In,Ga)(S,Se)<sub>2</sub> thin film solar cells via drop-on-demand inkjet printing. *Energy Environ. Sci.* **2016**, *9*, 2037–2043. [[CrossRef](#)]
11. Xin, H.; Katahara, J.K.; Braly, I.L.; Hillhouse, H.W. 8% Efficient Cu<sub>2</sub>ZnSn(S,Se)<sub>4</sub> Solar Cells from Redox Equilibrated Simple Precursors in DMSO. *Adv. Energy Mater.* **2014**, *4*, 1301823. [[CrossRef](#)]
12. Haass, S.G.; Diethelm, M.; Werner, M.; Bissig, B.; Romanyuk, Y.E.; Tiwari, A.N. 11.2% Efficient Solution Processed Kesterite Solar Cell with a Low Voltage Deficit. *Adv. Energy Mater.* **2015**, *5*, 1500712. [[CrossRef](#)]
13. Wang, W.; Winkler, M.T.; Gunawan, O.; Gokmen, T.; Todorov, T.K.; Zhu, Y.; Mitzi, D.B. Device Characteristics of CZTSSe Thin-Film Solar Cells with 12.6% Efficiency. *Adv. Energy Mater.* **2014**, *4*, 1301465. [[CrossRef](#)]
14. Schnabel, T.; Abzieher, T.; Friedlmeier, T.M.; Ahlswede, E. Solution-Based Preparation of Cu<sub>2</sub>ZnSn(S,Se)<sub>4</sub> for Solar Cells-Comparison of SnSe<sub>2</sub> and Elemental Se as Chalcogen Source. *IEEE J. Photovolt.* **2015**, *5*, 670–675. [[CrossRef](#)]
15. Stanchik, A.V.; Gremenok, V.F.; Juskenas, R.; Tyukhov, I.I.; Tivanov, M.S.; Fettkenhauer, C.; Shvartsman, V.V.; Giraitis, R.; Hagemann, U.; Lupascu, D.C. Effects of selenization time and temperature on the growth of Cu<sub>2</sub>ZnSnSe<sub>4</sub> thin films on a metal substrate for flexible solar cells. *Sol. Energy* **2019**, *178*, 142–149. [[CrossRef](#)]
16. Zhao, Y.; Han, X.; Chang, L.; Dong, C.; Li, J.; Yan, X. Effects of selenization conditions on microstructure evolution in solution processed Cu<sub>2</sub>ZnSn(S,Se)<sub>4</sub> solar cells. *Sol. Energy Mater. Sol. Cells* **2019**, *195*, 274–279. [[CrossRef](#)]
17. Yao, L.; Ao, J.; Jeng, M.J.; Bi, J.; Gao, S.; He, Q.; Zhou, Z.; Sun, G.; Sun, Y.; Chang, L.B.; et al. CZTSe solar cells prepared by electrodeposition of Cu-Sn-Zn stack layer followed by selenization at low Se pressure. *Nanoscale Res. Lett.* **2014**, *9*, 678. [[CrossRef](#)] [[PubMed](#)]
18. Jiang, J.; Yu, S.; Gong, Y.; Yan, W.; Zhang, R.; Liu, S.; Huang, W.; Xin, H. 10.3% Efficient CuIn(S,Se)<sub>2</sub> Solar Cells from DMF Molecular Solution with the Absorber Selenized under High Argon Pressure. *Sol. RRL* **2018**, *2*, 1800044. [[CrossRef](#)]
19. Clark, J.A.; Uhl, A.R.; Martin, T.R.; Hillhouse, H.W. Evolution of Morphology and Composition during Annealing and Selenization in Solution-Processed Cu<sub>2</sub>ZnSn(S,Se)<sub>4</sub>. *Chem. Mater.* **2017**, *29*, 9328–9339. [[CrossRef](#)]

20. Scragg, J.J.; Watjen, J.T.; Edoff, M.; Ericson, T.; Kubart, T.; Platzer-Bjorkman, C. A detrimental reaction at the molybdenum back contact in  $\text{Cu}_2\text{ZnSn}(\text{S,Se})_4$  thin-film solar cells. *J. Am. Chem. Soc.* **2012**, *134*, 19330–19333. [[CrossRef](#)]
21. Jeon, J.O.; Lee, K.D.; Seul Oh, L.; Seo, S.W.; Lee, D.K.; Kim, H.; Jeong, J.H.; Ko, M.J.; Kim, B.; Son, H.J.; et al. Highly efficient copper-zinc-tin-selenide (CZTSe) solar cells by electrodeposition. *ChemSusChem* **2014**, *7*, 1073–1077. [[CrossRef](#)] [[PubMed](#)]
22. Shin, B.; Bojarczuk, N.A.; Guha, S. On the kinetics of  $\text{MoSe}_2$  interfacial layer formation in chalcogen-based thin film solar cells with a molybdenum back contact. *Appl. Phys. Lett.* **2013**, *102*, 091907. [[CrossRef](#)]
23. Bucherl, C.N.; Oleson, K.R.; Hillhouse, H.W. Thin film solar cells from sintered nanocrystals. *Curr. Opin. Chem. Eng.* **2013**, *2*, 168–177. [[CrossRef](#)]
24. Weber, A.; Mainz, R.; Schock, H.W. On the Sn loss from thin films of the material system Cu–Zn–Sn–S in high vacuum. *J. Appl. Phys.* **2010**, *107*, 013516. [[CrossRef](#)]
25. Bree, G.; Coughlan, C.; Geaney, H.; Ryan, K.M. Investigation into the Selenization Mechanisms of Wurtzite CZTS Nanorods. *ACS Appl. Mater. Interfaces* **2018**, *10*, 7117–7125. [[CrossRef](#)] [[PubMed](#)]
26. Holzwarth, U.; Gibson, N. The Scherrer equation versus the ‘Debye-Scherrer equation’. *Nat. Nanotechnol.* **2011**, *6*, 534. [[CrossRef](#)] [[PubMed](#)]
27. Gokmen, T.; Gunawan, O.; Todorov, T.K.; Mitzi, D.B. Band tailing and efficiency limitation in kesterite solar cells. *Appl. Phys. Lett.* **2013**, *103*, 103506. [[CrossRef](#)]
28. Temgoua, S.; Bodeux, R.; Naghavi, N. Influence of the annealing atmosphere and precursor’s thickness on the properties of CZTSSe based solar cells. *Sol. Energy Mater. Sol. Cells* **2019**, *191*, 123–132. [[CrossRef](#)]



© 2019 by the authors. Licensee MDPI, Basel, Switzerland. This article is an open access article distributed under the terms and conditions of the Creative Commons Attribution (CC BY) license (<http://creativecommons.org/licenses/by/4.0/>).